

This document is the Accepted Manuscript version of a Published Work that appeared in final form in ACS Nano, copyright © American Chemical Society after peer review and technical editing by the publisher. To access the final edited and published work see: <https://doi.org/10.1021/acsnano.6b08176>

Poly(3-hexylthiophene) Nanoparticles Containing Thiophene-*S,S*-dioxide: Tuning of Dimensions, Optical and Redox Properties and Charge Separation Under Illumination

Francesca Di Maria^{§*}, Alberto Zanelli[§], Andrea Liscio^{§†}, Alessandro Kovtun[§], Elisabetta Salatelli[±], Raffaello Mazzaro^{#||}, Vittorio Morandi[#], Giacomo Bergamini^{||}, Avshalom Shaffer[¥] and Shlomo Rozen[¥]

§ CNR-ISOF, Via P. Gobetti 101, I-40129 Bologna, Italy

† CNR-ISC, Via Fosso del Cavaliere 100, I-00133 Roma, Italy

± Dpt. of Industrial Chemistry Toso Montanari, University of Bologna, Viale del Risorgimento 4, I-40136 Bologna, Italy

|| Dpt. of Chemistry Giacomo Ciamician, University of Bologna, Via Selmi 2, I-40126 Bologna, Italy

CNR-IMM, Via P. Gobetti 101, I-40129 Bologna, Italy

¥ School of Chemistry, Tel-Aviv University, 69978 Tel-Aviv, Israel

KEYWORDS: Polythiophene-*S,S*-dioxide, Rozen's reagent, organic nanoparticles, core-shell nanoparticles, heterojunction, Kelvin Probe, X-ray Photoelectron Spectroscopy.

ABSTRACT

We describe the preparation of poly(3-hexylthiophene-*S,S*-dioxide) nanoparticles using Rozen's reagent - $\text{HOF} \cdot \text{CH}_3\text{CN}$ - either on poly(3-hexylthiophene) (P3HT) or on preformed P3HT nanoparticles (P3HT-NPs). In the latter case core-shell nanoparticles (P3HT@PTDO-NPs) are formed, as confirmed by X-ray Photoelectron Spectroscopy measurements indicating the presence of oxygen on the outer shell. The different preparation modalities lead to a fine tuning of the chemical-physical properties of the nanoparticles. We show that absorption and photoluminescence features, electrochemical properties, size and stability of colloidal solutions can be finely modulated by controlling the amount of oxygen present. Atomic Force Microscopy measurements on the nanoparticles obtained by nanoprecipitation method from preoxidized P3HT (PTDO-NPs), display spherical morphology and dimensions down to 5 nm. Finally, Kelvin Probe measurements show that the coexistence of p- and n-type charge carriers in all types of oxygenated nanoparticles makes them capable to generate and separate charge under illumination. Furthermore, in core-shell nanoparticles the nanosegregation of the two materials, in different region of the nanoparticles, allows a more efficient charge separation.

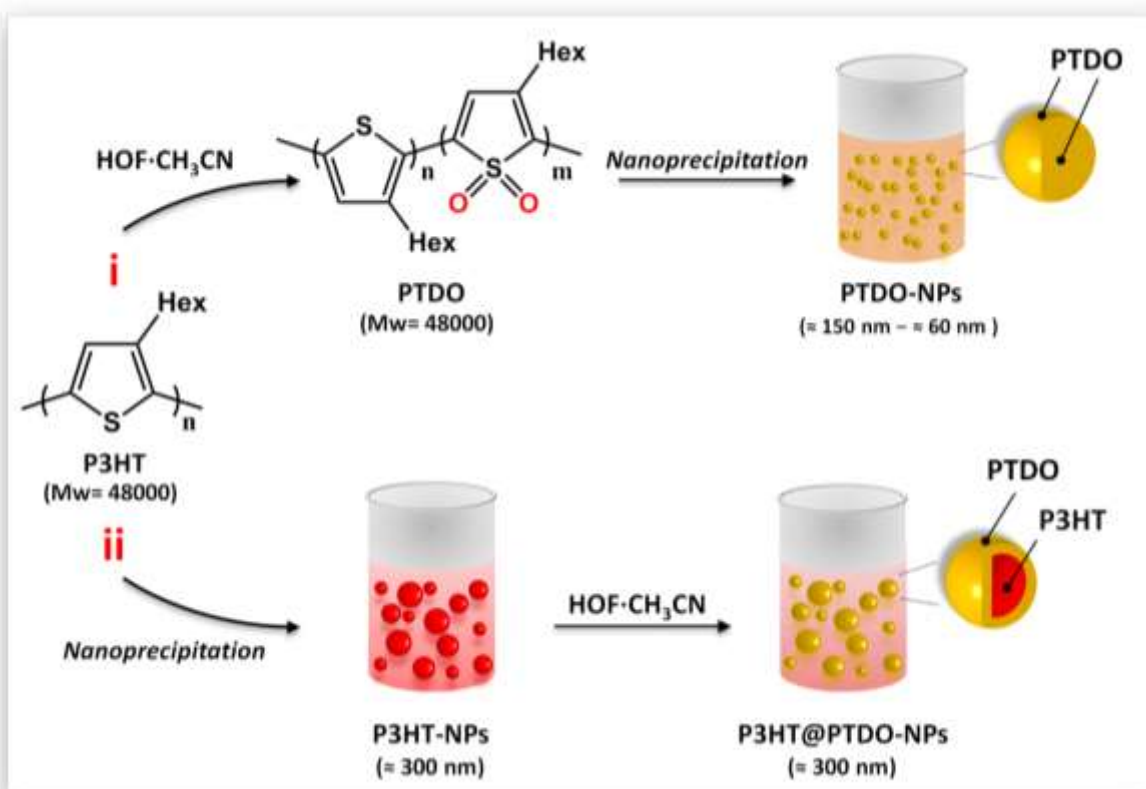
Currently, there is great interest in thiophene based materials functionalized at the sulfur atom with oxygen originating from the fact that the controlled introduction in oligo- and polythiophenes of thiophene *S,S*-dioxide moieties (TDO), both in sequence and number, allows for a wide tuning

of their optical and electronic properties.¹⁻⁶ In addition, the recent development of simple methods for their preparation has enabled the synthesis of unexplored families of sulfur-oxygenated oligo- and polythiophenes with potential applications spanning from organic electronics to chemical biology.⁷⁻¹⁹ The incorporation of strong electron acceptor TDO moieties deeply affects the HOMO-LUMO energy levels of the material causing a substantial reduction of the energy gap.²⁰⁻²⁴ Moreover, it may induce a change in the charge transport properties from p- to n-type,^{7,10,25} as well as in the self-assembly properties due to additional intra- and intermolecular hydrogen non-bonding interactions.²⁶ Recently, Campos *et al.* have proven that the presence of TDO moieties in polythiophenes causes a highly efficient intramolecular singlet fission process, favored by strong intramolecular donor-acceptor interactions, making these compounds very interesting candidates for third generation solar devices.^{2,4} In this framework it is challenging to introduce TDO units into nanostructured thiophene based materials, in particular nanoparticles, in order to get a wider tuning of their (opto)electronic properties. Indeed, nanoparticles based on conjugated polymers are emerging as multifunctional nanoscale materials that promise great potentials.²⁷⁻³³ Here we report that the use of Rozen's reagent, one of the most powerful oxygen transfer agents,⁸⁻¹¹ allows for the preparation of poly(3-hexylthiophene-*S,S*-dioxide) nanoparticles, whose properties can be skillfully tuned through the controlled introduction of TDO moieties before or after the formation of poly(3-hexylthiophene) nanoparticles. The different modalities of introduction of TDO moieties causes the formation of either PTDO-NPs obtained from pre-oxygenated P3HT, with dimensions down to 5 nm, or core-shell P3HT@PTDO-NPs obtained from oxygenation of the surface of preformed P3HT nanoparticles. We demonstrate that a fine modulation of the optical and electrochemical properties, photoinduced charge separation as well as dimensions and stability of the colloidal suspensions of TDO-nanoparticles can be achieved through the control of the

oxygenation degree. In core-shell P3HT@PTDO-NPs the precise confinement of the two materials with different semiconductor behavior – poly(3-hexylthiophene) and poly(3-hexylthiophene-*S,S*-dioxide) (PTDO) – allows the formation of innovative organic p-n junction nanoparticles as indicated by Kelvin Probe measurements (KP).

RESULTS AND DISCUSSION

Nanoparticles Preparation. Scheme 1 illustrates the strategy followed to prepare nanoparticles containing thiophene-*S,S*-dioxide units (TDO).











Scheme 1. Different strategies combining Rozen's reagent ($\text{HOF}\cdot\text{CH}_3\text{CN}$) and nanoprecipitation techniques to get well-defined functionalized TDO-nanoparticles: i) PTDO-NPs ii) *core-shell* P3HT@PTDO-NPs.

We prepared surfactant free oxygenated nanoparticles in two different ways: i) by previous oxygenation of P3HT with Rozen's reagent and subsequent formation of nanoparticles through nanoprecipitation (PTDO-NPs) or ii) by post-functionalization of pre-formed P3HT-NPs (*core-shell* P3HT@PTDO-NPs). Noticeably, while in PTDO-NPs the oxidized units are located randomly in the whole volume of the NPs, in *core-shell* P3HT@PTDO-NPs the TDO units are confined in the outer layer of the nanoparticles. In the latter case the presence of two different semiconducting thiophene based materials in two distinct regions of the nanoparticles, PTDO in the outer layer and P3HT in the inner core, leads to the formation of *all-thiophene core-shell* nanoparticles. Employing method i) we prepared three different types of PTDO-NPs, namely PTDO_{0.25}-NPs, PTDO_{0.5}-NPs and PTDO₁-NPs, through nanoprecipitation method^{34,35} starting from P3HT oxidized (PTDO) with different amounts of $\text{HOF}\cdot\text{CH}_3\text{CN}$ (0.25, 0.5 and 1 equivalents per thiophene units). Employing method ii) we prepared three different types of *core-shell* P3HT@PTDO-NPs, namely P3HT@PTDO_{0.25}-NPs, P3HT@PTDO_{0.5}-NPs and P3HT@PTDO₁-NPs, through addition of respectively 0.25, 0.5 and 1 equivalents of $\text{HOF}\cdot\text{CH}_3\text{CN}$ to a suspensions of preformed P3HT nanoparticles. P3HT was synthesized *via* oxidative polymerization with FeCl_3 (see SI) and the resulting crude product was first extracted with 2% aqueous HCl and then purified by Soxhlet extraction to ensure removal of iron.

Characterization. The size distribution of the different nanoparticles was investigated by Dynamic Light Scattering (DLS), Scanning Electron Microscopy (SEM), Transmission Electron

Microscopy (TEM) and Atomic Force Microscopy (AFM). Nanoparticles are spherical as shown by SEM and TEM images (Fig. 1 and S3-S6). The hydrodynamic size distributions of the nanoparticles measured by DLS reveal that the degree of oxygenation of the polymer has a considerable effect on the aggregation modalities during the formation of the nanoparticles (nanoprecipitation step). Indeed, as reported in Table 1, the dimensions of PTDO-NPs are smaller than those formed by pristine P3HT (P3HT-NPs) and become smaller and smaller as the oxygenation degree of the polymer increases (PTDO_{0.25}-NPs > PTDO_{0.5}-NPs > PTDO₁-NPs), ranging between ≈ 300 nm in the case of P3HT-NPs and ≈ 60 nm in PTDO₁-NPs.

Table 1. Dimensions and Z-potentials of P3HT-NPs, PTDO-NPs and P3HT@PTDO-NPs.

Nanoparticles	Hydrodynamic diameter (nm)		Z-potential (mV)
P3HT-NPs	298 ± 26		-38.1 ± 1.8
<i>PTDO-NPs</i>			
PTDO _{0.25} -NPs	153 ± 34		-30.7 ± 2.2
PTDO _{0.5} -NPs	94 ± 26		-32.2 ± 2.1
PTDO ₁ -NPs	63 ± 16		-36.4 ± 2.2
<i>core-shell NPs</i>			
P3HT@PTDO _{0.25} -NPs	297 ± 27		-48.6 ± 2.5
P3HT@PTDO _{0.5} -NPs	301 ± 28		-70.4 ± 2.6
P3HT@PTDO ₁ -NPs	299 ± 26		-75.8 ± 2.6

It is noteworthy to highlight that the size effect is not due to a reduction of the polymers chain length being obtained by the same P3HT batch. Measurements of particle size distributions performed by TEM and SEM on PTDO-NPs (Fig. 1Aa, S4 and S6) show the same trend observed by DLS indicating that the particles maintain the same shape and size in vacuum environments as

already observed for P3HT-NPs.³⁶ AFM measurements performed on the smallest PTDO₁-NPs revealed a broad (standard deviation / mean = 1.3) and high asymmetric (skewness = 3.1) diameter distribution (see SI for details) showing the presence of a long tail up to 140 nm. Moreover, very small nanoparticles till to 2 nm diameter (Fig.1Ab and S10) whose size is comparable to those of single chain polymer dots are observed.³⁷⁻⁴⁰ This suggests that the presence of oxygen atoms affects inter- and intramolecular interactions during particle formation leading to an increase in bending, torsion and folding of the polymer backbone. A different behavior is achieved when the oxygenation is carried out on pre-formed P3HT nanoparticles. Indeed, *core-shell* P3HT@PTDO-NPs display only very small size variations with respect to the starting P3HT nanoparticles (Table 1). In this case, shell formation does not affect the dimensions of the nanoparticles since the direct post-functionalization of preformed nanoparticles allows the nanoengineering of the surface of P3HT-NPs by grafting oxygen atoms directly on the external thiophene sulfur atoms. SEM, TEM and AFM images of *core-shell* P3HT@PTDO-NPs prove that the reaction between preformed P3HT-NPs and the oxidant (HOF·CH₃CN) does not alter their morphology (Fig. 1Bb, S3, S5, S6 and S9). The elemental mapping of the nanoparticles performed by STEM-EDS confirms the presence of C and S atoms for all the samples and, in particular, showing that the oxygen content is proportional to the degree of oxidation of the polymer (Fig. S7, S8). The oxidation of the thiophene sulfur atom is confirmed by infrared (IR) and X-ray photoelectron (XPS) spectroscopies. Infrared absorption spectra performed on both PTDO-NPs and P3HT@PTDO-NPs (Fig. 1Ac and S2) show the appearance of distinctive peaks at 1320 cm⁻¹ and 1146 cm⁻¹- characteristic of asymmetric and symmetric stretching of S-S dioxide group in thiophene derivatives^{7,19} - that progressively increase in intensity with increasing nanoparticles oxygenation, confirming that the oxidation takes place at the sulfur position. Moreover, XPS measurements on P3HT-NPs and *core-*

shell P3HT@PTDO-NPs (Fig. 1Bc) show that while S 2p spectrum of P3HT-NPs (black dots) displays only one peak at 164.0 ± 0.2 eV of binding energy corresponding to the S-C bond,⁴¹ S 2p spectrum of *core-shell* P3HT@PTDO-NPs (red dots) displays three peaks centered at different binding energies: 169.5 ± 0.2 , 164.4 ± 0.2 and 161.2 ± 0.2 eV respectively, indicating the presence of three non equivalent sulfur atoms. As previously reported, the lowest binding energy peak at 161.2 eV is ascribed to the metal-sulfur interaction⁴² while the other located to highest binding energy peak at 169.5 eV correspond to the oxidation of the thiophene sulfur atom (SO₂).^{43,44}

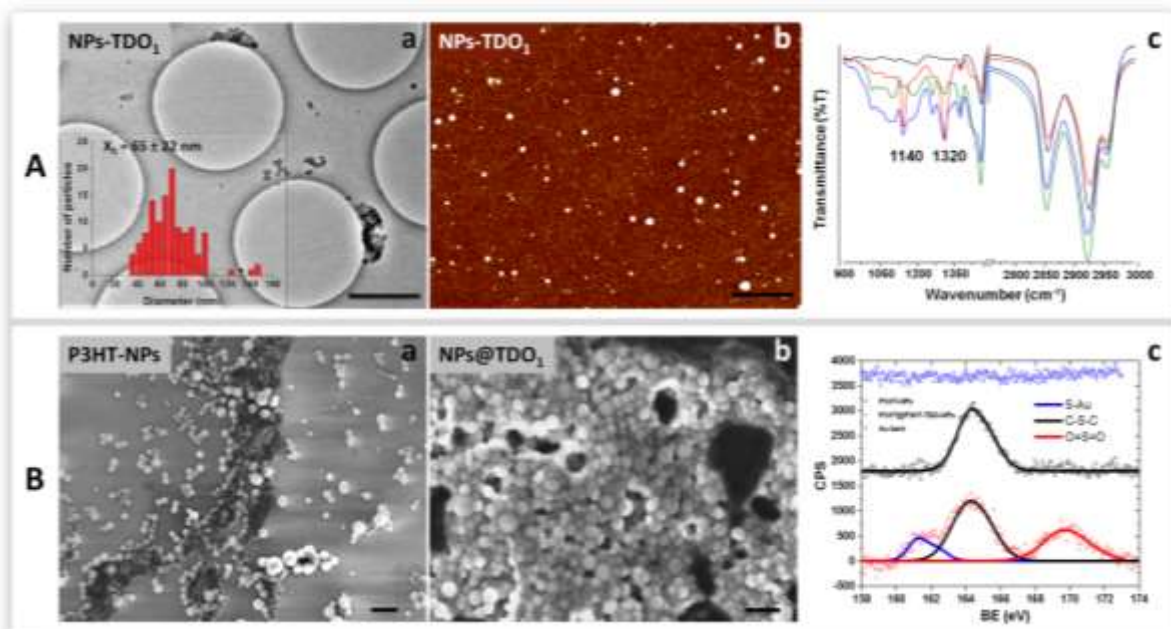


Figure 1. A) (a) Low magnification TEM micrograph of PTDO₁-NPs sample and in the inset its particle size histogram; (b) AFM image of PTDO₁-NPs; (c) Infrared spectra in the region between 900-1400 cm⁻¹ and 2750-3000 cm⁻¹ of PTDO-NPs (PTDO_{0.25}-NPs green line, PTDO_{0.5}-NPs blue line and PTDO₁-NPs red line) compared to P3HT-NPs (black line). B) SEM image of P3HT-NPs (a) and P3HT@PTDO₁-NPs (b) obtained after addition of 1 equivalent of HOF·CH₃CN to P3HT-NPs; (c) XPS of P3HT-NPs (□) and P3HT@PTDO₁-NPs (○). Scale bare, 1 μm.

Zeta potential values of all nanoparticles, reported in Table 1, indicate that the progressive increase of TDO units determines a simultaneous increase of the stability of the nanoparticles suspensions, showing very-long stability for months without any aggregation or precipitation. Noteworthy the oxygenation of the outer layer of P3HT nanoparticles (P3HT@PTDO-NPs) brings about a remarkable increase of the zeta potential value: from -38.10 mV up to -75.80 mV.

Optical properties. All oxygenated NPs were characterized by UV-Vis and photoluminescence spectroscopy and compared to the corresponding polymers in solution. In Figure 2 we report the absorption and emission spectra of polymers P3HT, PTDO_{0.25}, PTDO_{0.5} and PTDO₁ in dichloromethane solution (Fig. 2A) and as nanoparticles dispersed in water (Fig. 2B).

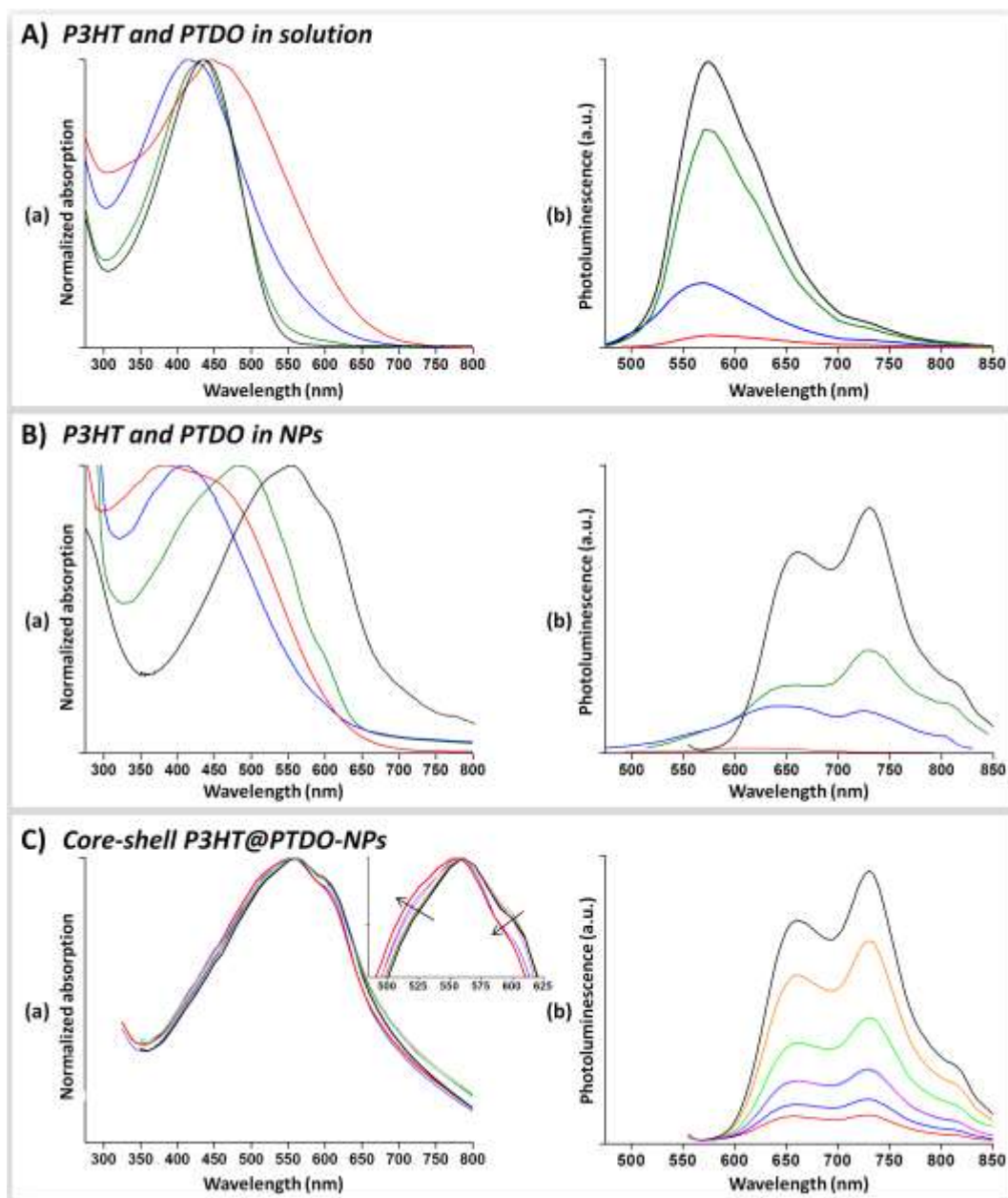


Figure 2. A), B) Normalized absorption (a) and emission spectra (b) of P3HT (black line) and oxygenated P3HT in different ratio (green: PTDO_{0.25}, Blue: PTDO_{0.5}; red: PTDO₁) in CH₂Cl₂ solution and as nanoparticles suspended in water (Black: P3HT-NPs, green PTDO_{0.25}-NPs, Blue: PTDO_{0.5}-NPs; red: PTDO₁-NPs). C) Normalized absorption (a) and emission spectra (b) of *core-shell* P3HT@PTDO-NPs obtained upon addition of increasing amount of HOF·CH₃CN to a suspension of P3HT-NPs.

In solution, the progressive increase of TDO units from P3HT to PTDO₁ (Fig. 2Aa) induces a widening of the absorption bands, due to the random oxygenation,⁶ accompanied by a gradual red shift of the optical absorption onset (E_g^{opt}) in agreement with the electrochemical data (see below). Furthermore, the increased oxygenation causes a progressive quenching of the fluorescence (Fig. 2Ab) in the order PTDO₁ > PTDO_{0.5} > PTDO_{0.25} > P3HT. This result concurs with previous measurements we performed on oligo- and polythiophenes containing TDO units,⁷ where the deactivation process of the excited singlet state S₁, rather than proceeding through fluorescence or ISC occurs through a competitive and more rapid process leading to the formation of low-energy dark states and low-energy triplet states.^{6,7,45} Differently from the solution, the aggregation of P3HT in nanoparticles determines a well-structured and strong red-shifted band both in absorption and emission spectra (Fig. 2Ba, 2Bb black line), attributable to a higher degree of intra- and interchain order.^{36,46,47} As shown in Figure 2B, going from P3HT-NPs to the more oxygenated PTDO-NPs, a blue-shift in the maximum of the absorption spectra (Fig. 2Ba) and a progressive decrease in the intensity of the fluorescence emission (Fig. 2Bb) are observed. This observed blue shift is consistent with the smaller size of PTDO-NPs in which the polymer is more twisted thus decreasing the effective conjugation length. In agreement, a smaller scattering in the absorption spectra of PTDO-NPs is also observed. Figure 2C shows the absorption and emission spectra of the *core-shell* P3HT@PTDO-NPs. In this case the oxygenation of P3HT-NPs is limited to the outer layer (shell) and increasing amounts of TDO units on it slightly affects the UV-Vis absorption spectra – which remains similar to that of the starting nanoparticles with only a small change in the intensity of the vibronic peaks (A_{00}/A_{02}) – indicating that the organization of P3HT in the NPs does not change after oxygenation with HOF·CH₃CN. On the other hand, the emission progressively vanishes confirming that the surface of the P3HT nanoparticles is markedly altered.

It is noteworthy that the gradual increase of TDO units on the outer shell of P3HT nanoparticles causes a change in the excited state lifetimes (Table 2).

Table 2. Lifetime of P3HT-NPs, PTDO-NPs and P3HT@PTDO-NPs

Nanoparticles	t_1 (405 nm)	t_2 (405 nm)
P3HT-NPs	0.34	1.15
<i>PTDO-NPs</i>		
PTDO _{0.25} -NPs	0.16	1.17
PTDO _{0.5} -NPs	0.13	1.15
PTDO ₁ -NPs	-	-
<i>Core-shell NPs</i>		
P3HT@PTDO _{0.25} -NPs	0.22	1.16
P3HT@PTDO _{0.5} -NPs	0.18	1.18
P3HT@PTDO ₁ -NPs	0.16	1.15

Within the *core-shell* P3HT@PTDO-NPs series, going to the more oxygenated nanoparticles (P3HT@TDO₁-NPs), we observe that the short-time decay component (t_1) undergoes a progressive decrease⁴ – from 0.34 ns to 0.16 ns – becoming coincident to that detected in PTDO-NPs (0.13-0.16 ns), while the long-time decay component (t_2) remains unchanged as in P3HT-NPs (1.5 ns). We hypothesize that the long-time decay components t_2 , which is not affected by the number of TDO units on the surface, is characteristic of the internal structure of the nanoparticles (*core*) thus dependent on the type of aggregation and crystallinity,^{48,49} while the short-time decay t_1 , being influenced by the oxygenation degree, is probably characteristic of P3HT chains near the outer layer of the NPs (*shell*).

Cyclic voltammetry. In Table 3 we report the oxidation and reduction potentials, HOMO-LUMO energy levels⁵⁰ and energy gaps (E_g^{elect}) of P3HT-NPs, PTDO-NPs and *core-shell*

P3HT@PTDO-NPs compared with the potentials of cast films of the polymers used for their preparation.

Table 3. Redox potentials of cast films of P3HT, PTDO, P3HT-NPs, PTDO-NPs and P3HT@PTDO-NPs

Materials	E^{ox} (V vs. SCE)	E^{red} (V vs. SCE)	E_g (eV)	HOMO (eV)	LUMO (eV)
<i>P3HT Polymer and NPs</i>					
P3HT-NPs	0.73	-1.94	2.67	5.41	2.74
P3HT*	1.02	≤ -1.8	≥ 2.82	5.70	≤ 2.88
<i>PTDO Polymers and NPs</i>					
PTDO _{0.25} -NPs	0.77	-1.50	2.27	5.45	3.18
PTDO _{0.25} *	1.07	≤ -1.8	≥ 2.87	5.75	≤ 2.88
PTDO _{0.5} -NPs	0.90	-0.88	1.78	5.58	3.80
PTDO _{0.5} *	1.12	-0.96	2.08	5.80	3.72
PTDO ₁ -NPs	0.97	-0.57	1.54	5.65	4.11
PTDO ₁ *	1.25	-0.75	2.00	5.93	3.93
<i>Core-shell NPs</i>					
P3HT@PTDO _{0.25} -NPs	0.75	n.d.	-	5.43	-
P3HT@PTDO _{0.5} -NPs	0.79	-0.94	1.73	5.47	3.74
P3HT@PTDO ₁ -NPs	0.78	-0.63	1.42	5.46	4.05

*deposited from CH₂Cl₂

Comparing the potentials of the cast films of PTDO-NPs with the cast films of their corresponding polymers (PTDO), it is evident that the structure/morphology has a remarkable influence on the electrochemical properties. In all cases, when the materials are organized into supramolecular ordered nanoparticles, a reduction of the energy gap (E_g), in the range of 0.15-0.60 eV, compared to the corresponding bulk materials is observed. The increasing number of thiophene-*S,S*-dioxides units into P3HT macromolecules (PTDO_{0.25}, PTDO_{0.5}, PTDO₁) and in their resulting nanoparticles (PTDO_{0.25}-NPs, PTDO_{0.5}-NPs, PTDO₁-NPs) causes a gradual increase of

the oxidation potentials (from 1.07 V to 1.25 V for the cast film of the oxygenated polymers and from 0.77 V to 0.97 V for the cast film of their corresponding NPs) and a significant decrease of the reduction potentials (from -1.50 V to -0.57 V and from ≤ -1.8 V to -0.75 V for the cast film of the polymers and NPs respectively), leading to low-bandgap polymers and nanoparticles. This noteworthy increase of the electron affinity and the reduction of the E_g value suggest an n-type semiconductor behavior for these materials, as we observed in a recent work with similar oxygenated polythiophenes.⁷ On the contrary, in *core-shell* nanoparticles the progressive oxygenation of the external layer induces a negligible variation of the oxidation potential (from 0.75 V to 0.78 V), remaining close to the oxidation potential of P3HT-NPs (0.73 V), and a significant shift of the reduction potential to less negative potentials (-0.94 V for P3HT@PTDO_{0.5}-NPs and -0.63 V for P3HT@PTDO₁-NPs) similar to those detected in PTDO-NPs. In agreement with the UV-PL measurements, these values confirm that only few layers are oxidized leaving the inner core of P3HT-NPs unchanged in its electrochemical properties. As a result a lowering of the energy gap of the *core-shell* nanoparticles (P3HT@PTDO₁-NPs, 1.42 eV) compared with the corresponding pure core (PTDO₁-NPs, 2.67 eV) and pure shell (P3HT-NPs, 1.54 eV) nanoparticles is observed (Fig. 3A, 3B).

Kelvin Probe measurements (KP). As observed for inorganic core-shell quantum dots,^{51,52} in these *entirely thiophenic core-shell* nanoparticles – made of (p-type) P3HT and (n-type) PTDO semiconducting layers – the different alignment of the energy levels between core and shell should be energetically favorable to promote the photogenerated charges in different regions of the nanoparticles (p-n heterojunction), thus determining a better charge separation (Fig. 3B). To confirm this hypothesis and to corroborate the n-type semiconductor behavior both in *core-shell* P3HT@PTDO-NPs and PTDO-NPs, Kelvin Probe (KP) measurements were carried out. KP is a

powerful tool that allows to visualize the photogeneration and splitting of charges in nano-objects – having both electron acceptor and electron donor properties – through measurement of the electric potential at the surface (SP) resulting from the interaction between the tip and the sample.⁵³⁻⁵⁵ Surface photovoltage (SPV), defined as the difference between the surface potential under illumination and in the dark, provides information about the charging/discharging and defect states of surface of semiconducting materials. It is noteworthy to remind that the p-n junction is not directly accessible and that the measured SPV corresponds to the photoinduced charge density variation measured at the external surface. KP measurements are performed in dark and in steady-state condition upon illumination, consequently the measurement of the SPV is a time-average is due to charge separation at the interface in steady-state condition upon illumination. Moreover, we have to take into account that the sub-surface sensitivity of the techniques can range between few nm up to 100 nm,⁵⁶ which is comparable to the nanoparticle size. For this reason, the direct quantitative analysis of SPV is not trivial because it corresponds to the average value of all the excitation/de-excitation processes at the internal interface and the corresponding change of the charge density in the nanoparticle surface and bulk. As shown in Figure 3C, in *core-shell* P3HT@PTDO-NPs the charge density of the nanoparticles depends markedly on the degree of shell oxygenation. Going from P3HT-NPs to the oxygenated P3HT@PTDO_{0.5}-NPs the increase of the measured SPV value (up to 100 mV) corresponds to the ability of the *core-shell* P3HT@PTDO-NPs to better separate the charge compared to P3HT nanoparticles (Fig. 3C).

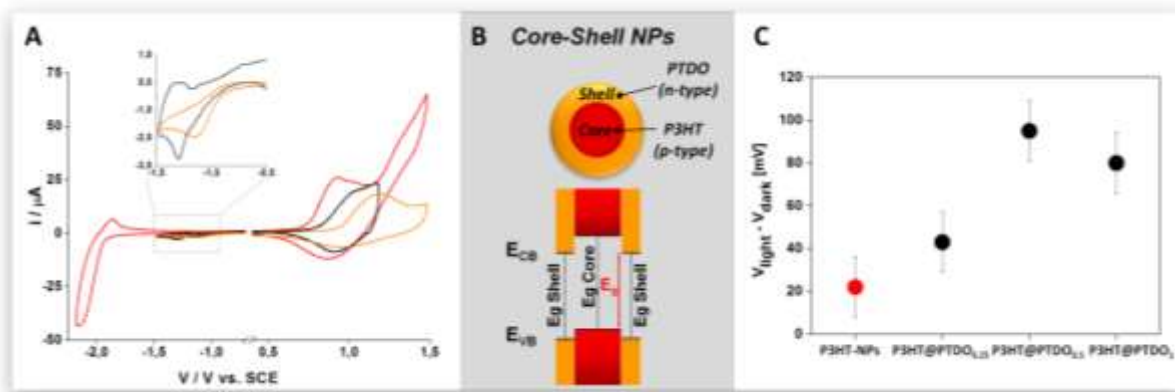


Figure 3. A) Cyclic voltammograms of P3HT-NPs (red line), P3HT@PTDO-NPs (black line) and PTDO-NPs (orange line); B) Schematic representation of the cross section of core-shell P3HT@PTDO-NPs made of PTDO in the shell and P3HT in the core and its corresponding Energy levels. C) Measured SPV values corresponding to different nanoparticles (red circle P3HT-NPs, black circle P3HT@PTDO-NPs).

Despite of a quantitative analysis of the SPV needs a dedicated study of the nanoparticles morphology (*i.e.* the diameter of the inner shell) and its dielectric properties, the measured positive value can be attributed to electron-hole (polaron) pairs in n-type semiconductor that are polarized by a space charge layer. Increasing the oxidation degree, the achieved SPV reaches an asymptotic value. Indeed, the potential measured on P3HT@PTDO_{0.5}-NPs and P3HT@PTDO₁-NPs remains approximately the same suggesting that once reached a threshold of oxygenation in the outer layer no better charge separation is observed. In PTDO-NPs we found a similar behavior (Fig. S11), even though the difference in SPV observed between PTDO₁-NPs and PTDO_{0.25}-NPs is lower (≈ 20 mV) than that measured between P3HT@PTDO₁-NPs and P3HT@PTDO_{0.25}-NPs (≈ 60 mV) indicating that the presence of the TDO units has a higher effect on surface photovoltage response when they are confined on the outer layer.

CONCLUSIONS

We have successfully demonstrated that the chemical strategy used in this work allows the preparation of poly(3-hexylthiophene) nanoparticles containing thiophene-*S,S*-dioxide units (TDO) located either on the outer layer of the NPs (hence forming all-organic *core-shell* nanoparticles) or randomly distributed in the volume of the NPs. We show that through controlled insertion of TDO moieties it is possible to achieve a fine tuning of NPs size (which can be scaled down to 5nm) and of NPs chemical-physical properties such as a markedly low-lying LUMO (in the range 0.5-0.9 eV), a very low energy gap (1.43 eV) and a change from p- to n-type semiconducting behavior (as inferred from Kelvin Probe measurements). We demonstrate that the coexistence of p- and n-type charge carriers in TDO containing nanoparticles allows for a marked charge separation under illumination, suggesting potential application in photovoltaic devices. Finally, we believe that our chemical strategy based on the use of Rozen's reagent represents a simple way for the preparation of thiophene-based nanoparticles with p/n junctions. Moreover, due to its extreme versatility and easy operative conditions, this strategy could be extended to other types of supramolecular ordered nanostructures made of potentially oxidizable organic materials, enabling the fabrication of advanced multifunctional nanostructures.

METHODS

All chemicals and dialysis sack (MWCO 12,000 Da) were purchased from Sigma-Aldrich and used as received. ¹H-NMR spectra were recorded on Bruker DRX 400 spectrometer. Uv-vis absorption spectra were taken on a Agilent Technologies CARY 100 UV-Vis spectrophotometer and on a SpectraMax® i3x Multi-Mode Detection Platform, Molecular Devices; Photoluminescence spectra were collected on a Perkin Elmer LS50 spectrofluorometer and on a

SpectraMax® i3x Multi-Mode Detection Platform, Molecular Devices. Fluorescence measurements were performed using an excitation wavelength corresponding to the maximum absorption lambda. Infrared (IR) spectra were obtained using a Bruker Tensor 27 FT-IR. Gel permeation chromatography (GPC) was carried out on a HPLC Lab Flow 2000 apparatus, equipped with an injector Rheodyne 7725i, a Phenomenex Phenogel Mixed 5µ MXM and MXL columns and a UV-vis detector Linear Instruments model UVIS-200, working at 254nm, using THF as the eluent. Molecular weights (MWs) and polydispersity indices (Đ) are reported relative to polystyrene standards.

Preparation of Rozen's reagent. Rozen's reagent was synthesized according to a reported procedure, using F₂.^{57,58} A general scheme and further details for its preparation are reported in Supporting Information.

Synthesis and characterization of the polymers. Full details of the synthesis and characterization of the poly(3-hexylthiophene) (P3HT) and oxygenated poly(3-hexylthiophene) (PTDO) are given in Supporting Information.

Preparation of P3HT- and PTDO-NPs: P3HT nanoparticles were obtained by using the nanoprecipitation method. A sample of poly(3-hexylthiophene) (5 mg) was dissolved in THF (200 µL) and then was slowly injected into 5 mL of deionized water at room temperature and under vigorous stirring. Finally, the colloidal suspension formed was filtered through a paper filter (whatmann grade 4) and then was dialyzed in water, which was changed three times a day, to remove the organic solvent. PTDO-NPs were prepared using the same procedure employed for the preparation of P3HT-NPs starting from PTDO.

Preparation of core-shell P3HT@PTDO-NPs: to a colloidal suspensions of P3HT-NPs increasing amounts of HOF·CH₃CN (0.25, 0.5 and 1 equivalents) were slowly added and the

resulting solutions were stirred for 20 min at room temperature. Finally, to neutralize the reaction the resulting solutions were dialyzed in water.

Dynamic light scattering (DLS) measurements. DLS measurements were performed with a Nanobrook Omni Particle Size Analyzer, with a wavelength of 659 nm in backscattering mode. Nanoparticles were dispersed in deionized water during analysis and measurements were taken at 25°C. Zeta potential measurements were performed using Smoluchowski equation.

Scanning Electron Microscopy (SEM) and Transmission Electron Microscopy (TEM). SEM images were collected with a SEM-FEG Zeiss LEO 1530 operating at $V_{\text{acc}} = 5$ keV. The samples were drop casted onto Si/SiO₂ wafers and dried under vacuum with no further treatment. HRTEM and STEM micrographs were taken on a FEI Tecnai F20 TEM equipped with a Schottky emitter operating at 120 kV. The samples were drop casted onto Quantifoil carbon coated TEM grids and dried under vacuum overnight.

Atomic Force Microscopy (AFM) measurements. AFM measurements were performed with tapping-mode atomic force microscopy (tp-AFM). Both topographic and phase-contrast images were acquired in air by employing a commercial microscope NTEGRA Aura (NT-MDT) and using ($k=40 \text{ N}\cdot\text{m}^{-1}$) ultra-lever silicon tips (RTESPA-300, Bruker) with oscillating frequencies of about 300 KHz. NPs were deposited by spin coating (500 rpm) from water solution on ultraflat silicon substrate with thin native oxide film. Substrates were cleaned by 5' sonication in acetone, followed by 5' sonication in 2-propanol and 5' in air plasma treatment.

X-ray photoelectron spectroscopy (XPS) measurements. XPS spectra were recorded with a Phoibos 100 hemispherical energy analyzer (Specs) using Mg K_α radiation ($\hbar\omega = 1253.6$ eV). The X-ray power was 125 W. The spectra were recorded in the constant analyzer energy (CAE) mode with analyzer pass energies of 40 eV for the high resolution spectra. Charging effects were

corrected by energy calibration on Au 4f_{7/2} level relative to 84.0 eV. The base pressure in the analysis chamber during analysis was 5×10^{-10} mbar. All the spectra were normalized to the corresponding acquisition time. During this period no signal alteration was ever detected. High resolution XPS spectra of S 2p were analyzed by CasaXPS (Casa software, Ltd), the curve fitting was carried out using Gaussian/Lorentzian curves shape (GL(30)) with a full width half-maximum of 1.4 eV and for each peak S 2p doublet the spin orbit split was 1.2 eV (2p_{1/2}-2p_{3/2}). For each sample NPs were deposited on golden slides purchased from Arrandee (Germany) having the following specifications: Au, 250 nm thick and 2.5 nm of Cr, as adhesive layer. Gold substrates were cleaned using the protocol for silicon substrates. Samples were prepared drop-casting the NPs solutions on freshly cleaned golden slice and immediately put in High-Vacuum overnight. After, samples were heated in Ultra-High-Vacuum chamber at 80 °C for 1 hour in order to remove the residual water.

Kelvin Probe (KP) measurements. KP measurements were performed under ambient conditions using 2 mm diameter gold tip amplifier (Ambient Kelvin Probe Package from KP Technology Ltd.). KP technique provides a voltage resolution of about 5 mV on a sampled surface area of about 3 mm². Calibration of the probe was performed comparing two reference surfaces: aged gold and freshly cleaved High Oriented Pyrolytic Graphite. A comprehensive description of the technique can be found in references 54 and 55. For each sample NPs were deposited on golden slides purchased from Arrandee (Germany) having the following specifications: Au, 250 nm thick and 2.5 nm of Cr, as adhesive layer. Gold substrates were cleaned using the protocol for silicon substrates. NPs were deposited by spin coating (500 rpm) from water solution on ultraflat silicon substrate with thin native oxide film. Substrates were cleaned by 5' sonication in Acetone, followed by 5' sonication in 2-Propanol and 5' in air plasma treatment.

Quantum Yield (QY) measurements. Luminescent excited state lifetimes of the nanoparticles, in the range 0.2 ns to 1 μ s, were measured by an Edinburgh FLS920 spectrofluorometer equipped with a TCC900 card for data acquisition in time-correlated single-photon counting experiments (0.2 ns time resolution) with a LDH-P-C-405 pulsed diode laser.

Cyclic Voltammetry of polymers and nanoparticles. Cyclic voltammetries have been carried out at room temperature in anhydrous propylene carbonate (Sigma-Aldrich) with 0.1 mol·L⁻¹ (C₂H₅)₄NBF₄ (Fluka, puriss. vacuum dried) by using an AMEL electrochemical system model 5000. Working electrodes were Pt discs (diameter 1 mm) modified by drop casting of the polymer solutions or nanoparticles suspensions. Auxiliary electrode Pt wire and reference electrode aqueous KCl Saturated Calomel Electrode (SCE) were both separated from the working electrode compartment by a liquid bridge of the same electrolyte solution.

ASSOCIATED CONTENT

Supporting Information Synthetic details and characterization data. This material is available free of charge *via* the Internet at <http://pubs.acs.org>

AUTHOR INFORMATION

Corresponding Author

* E-mail: francesca.dimaria@isof.cnr.it

Notes

The authors declare no competing financial interest

ACKNOWLEDGMENTS

This research has received funding from the European Union H2020 Marie Skłodowska-Curie grant agreement No. 642196. Thanks are due to Simone Dell'Elce for AFM measurements. We are grateful to Dr. Giovanna Barbarella for helpful discussion.

REFERENCES

- (1) Dell, E. J.; Capozzi, B.; Xia, J.; Venkataraman, L.; Campos, L. M. Molecular Length Dictates the Nature of Charge Carriers in Single-Molecule Junctions of Oxidized Oligothiophenes. *Nat. Chem.* **2015**, *7*, 209–214.
- (2) Busby, E.; Xia, J.; Wu, Q.; Low, J. Z.; Song, R.; Miller, J. R.; Zhu, X. Y.; Campos, L. M.; Sfeir, M. Y. A Design Strategy for Intramolecular Singlet Fission Mediated by Charge-Transfer States in Donor-Acceptor Organic Materials. *Nat. Mater.* **2015**, *14*, 426–433.
- (3) Capozzi, B.; Xia, J.; Adak, O.; Dell, E. J.; Liu, Z. F.; Taylor, J. C.; Neaton, J. B.; Campos, L. M.; Venkataraman, L. Single-Molecule Diodes with High Rectification Ratios through Environmental Control. *Nat. Nanotechnol.* **2015**, *10*, 522–527.
- (4) Busby, E.; Xia, J.; Low, J. Z.; Wu, Q.; Hoy, J.; Campos, L. M.; Sfeir, M. Y. Fast Singlet Exciton Decay in Push-Pull Molecules Containing Oxidized Thiophenes. *J. Phys. Chem. B* **2015**, *119*, 7644–7650.
- (5) Dell, E. J.; Campos, L. M. T. The Preparation of Thiophene-*S,S*-dioxides and their Role in Organic Electronics. *J. Mater. Chem.* **2012**, *22*, 12945–12952.
- (6) Wei, S.; Xia, J.; Dell, E. J.; Jiang, Y.; Song, R.; Lee, H.; Rodenbough, P.; Briseno, A. L.; Campos, L. M. Bandgap Engineering through Controlled Oxidation of Polythiophenes. *Angew. Chem.* **2014**, *126*, 1863–1867.
- (7) Di Maria, F.; Zangoli, M.; Palam, I. E.; Fabiano, E.; Zanelli, A.; Monari, M.; Perinot, A.; Caironi, M.; Maiorano, V.; Maggiore, A.; *et. al.* Improving the Property-Function Tuning Range

of Thiophene Materials *via* Facile Synthesis of Oligo/Polythiophene-*S*-Oxides and Mixed Oligo/Polythiophene-*S*-Oxides/Oligo/Polythiophene-*S,S*-Dioxides. *Adv. Funct. Mat.* **2016**, *26*, 6970–6984.

(8) Rozen, S.; Bareket, Y. A Novel Oxidation of Thiophenes Using HOF·MeCN. *J. Chem. Soc., Chem. Commun.* **1994**, 1959–1959.

(9) Rozen, S.; Bareket, Y. Oxidation of Sulfur-Containing Compounds with HOF·CH₃CN. *J. Org. Chem.* **1997**, *62*, 1457–1462.

(10) Amir, E.; Rozen, S. Synthesis of [all]-*S,S*-Dioxide Oligothiophenes Using HOF·CH₃CN. *Angew. Chem. Int. Ed.* **2005**, *44*, 7374–7378.

(11) Rozen, S. HOF·CH₃CN: Probably the Best Oxygen Transfer Agent Organic Chemistry Has To Offer. *Acc. Chem. Res.* **2014**, *47*, 2378–2389.

(12) Chochos, C. L.; Tagmatarchis, N.; Gregoriou, V. G. Rational Design on n-Type Organic Materials for High Performance Organic Photovoltaics. *RSC Adv.* **2013**, *3*, 7160–7181.

(13) Sonar, P.; Lim, J. P. F.; Chan, K. L. Organic Non-Fullerene Acceptors for Organic Photovoltaics. *Energy Environ. Sci.* **2011**, *4*, 1558–1574.

(14) Osken, I.; Gundogan, A. S.; Tekin, E.; Eroglu, M. S; Ozturk, T. Fluorene-dithienothiophene-*S,S*-dioxide Copolymers. Fine-Tuning for OLED Applications. *Macromolecules* **2013**, *46*, 9202–9210.

(15) Ghofraniha, N.; Viola, I.; Di Maria, F.; Barbarella, G.; Gigli, G.; Conti, C. Random Laser from Engineered Nanostructures Obtained by Surface Tension Driven Lithography. *Laser Photonics Rev.* **2013**, *7*, 432–438.

(16) Verolet, Q.; Soleimanpour, S.; Fujisawa, K.; Dal Molin, M.; Sakai, N.; Matile, S. Design and Synthesis of Mixed Oligomers with Thiophenes, Dithienothiophene *S,S*-Dioxides,

Thieno[3,4]pyrazines and 2,1,3-Benzothiadiazoles: Flipper Screening for Mechanosensitive Systems. *ChemistryOpen* **2015**, *4*, 264–267.

(17) Palamà, I. E.; Di Maria, F.; D'Amone, S.; Barbarella, G.; Gigli, G. Biocompatible and Biodegradable Fluorescent Microfibers Physiologically Secreted by Live Cells Upon Spontaneous Uptake of Thiophene Fluorophore. *J. Mater. Chem. B* **2015**, *3*, 151–158.

(18) Palamà, I. E.; Di Maria, F.; Viola, I.; Fabiano, E.; Gigli, G.; Bettini, C.; Barbarella, G. Live-Cell-Permeant Thiophene Fluorophores and Cell-Mediated Formation of Fluorescent Fibrils. *J. Am. Chem. Soc.* **2011**, *133*, 17777–17785.

(19) Shefer, N.; Harel, T.; Rozen, S. Synthesis of Oxygenated Fused Oligothiophenes with $\text{HOF} \cdot \text{CH}_3\text{CN}$. *J. Org. Chem.* **2009**, *74*, 6993–6998.

(20) Barbarella, G.; Favaretto, L.; Zambianchi, M.; Pudova, O.; Arbizzani, C.; Bongini, A.; Mastragostino, M. From Easily Oxidized to Easily Reduced Thiophene-Based Materials. *Adv. Mater.* **1998**, *10*, 551–554.

(21) Barbarella, G.; Favaretto, L.; Sotgiu, G.; Zambianchi, M.; Antolini, L.; Pudova, O.; Bongini, A. Oligothiophene *S,S*-Dioxides. Synthesis and Electronic Properties in Relation to the Parent Oligothiophenes. *J. Org. Chem.* **1998**, *63*, 5497–5506.

(22) Bongini, A.; Barbarella, G.; Zambianchi, M.; Arbizzani, C.; Mastragostino, M. Thiophene *S*-Oxides: Orbital Energies and Electrochemical Properties. *Chem. Commun.* **2000**, 439–440.

(23) Antolini, L.; Tedesco, E.; Barbarella, G.; Favaretto, L.; Sotgiu, G.; Zambianchi, M.; Casarini, D.; Gigli, G.; Cingolani, R. Molecular Packing and Photoluminescence Efficiency in Odd-Membered Oligothiophene *S,S*-Dioxides. *J. Am. Chem. Soc.* **2000**, *122*, 9006–9013.

- (24) Tsai, C.; Chirdon, D. N.; Maurer, A. B.; Bernhard, S.; Noonan K. J. T. Synthesis of Thiophene 1,1-Dioxides and Tuning Their Optoelectronic Properties. *Org. Lett.* **2013**, *15*, 5230–5233.
- (25) Li, P.; Cui, Y.; Song, C.; Zhang, H. Effects of Sulfur Oxidation on the Electronic and Charge Transport Properties of Fused Oligothiophene Derivatives. *J. Phys. Chem. C* **2016**, *120*, 14484–14494.
- (26) Antolini, L.; Tedesco, E.; Barbarella, G.; Favaretto, L.; Sotgiu, G.; Zambianchi, M.; Casarini, D.; Gigli, G.; Cingolani, R. Molecular Packing and Photoluminescence Efficiency in Odd-Membered Oligothiophene *S,S*-Dioxides. *J. Am. Chem. Soc.* **2000**, *122*, 9006–9013.
- (27) Yao, W.; Zhao, Y. S. Tailoring the Self-assembled Structures and Photonic Properties of Organic Nanomaterials. *Nanoscale* **2014**, *6*, 3467–3476.
- (28) Pecher J.; Mecking S. Nanoparticles of Conjugated Polymers. *Chem. Rev.* **2010**, *110*, 6260–6279.
- (29) Millstone, J. E.; Kavulak, D. F. J.; Woo, C. H.; Holcombe, T. W.; Westling, E. J.; Briseno, A. L.; Toney, M. F.; Frechet, J. M. J. Synthesis, Properties, and Electronic Applications of Size-Controlled Poly(3-hexylthiophene) Nanoparticles. *Langmuir* **2010**, *26*, 13056–13061.
- (30) Gärtner, S.; Christmann, M.; Sankaran, S.; Röhm, H.; Prinz, E.; Penth, F.; Pütz, A.; Türel, A. E.; Penth, B.; Baumstümmler, B.; *et al.* Eco-Friendly Fabrication of 4% Efficient Organic Solar Cells from Surfactant-Free P3HT:ICBA Nanoparticle Dispersions. *Adv. Mater.* **2014**, *26*, 6653–6657.
- (31) Yang, K.; Xu, H.; Cheng, L.; Sun, C.; Wang, J.; Liu, Z. *In Vitro* and *In Vivo* Near-Infrared Photothermal Therapy of Cancer Using Polypyrrole Organic Nanoparticles. *Adv. Mater.* **2012**, *24*, 5586–5592.

- (32) Han, X.; Bag, M.; Gehan, T. S.; Venkataraman, D.; Maroudas D. Analysis of Charge Transport and Device Performance in Organic Photovoltaic Devices with Active Layers of Self-Assembled Nanospheres. *J. Phys. Chem. C* **2015**, *119*, 25826–25839.
- (33) Zucchetti, E.; Zangoli, M.; Bargigia, I.; Bossio, C.; Di Maria, F.; Barbarella, G.; D'Andrea, C.; Lanzani, G.; Antognazza, M. R. Poly(3-hexylthiophene) nanoparticles for biophotonics: study of the mutual interaction with living cells. *J. Mater. Chem. B*, **2017**, *5*, 565–574.
- (34) Shimizu, H.; Yamada, M.; Wada, R.; Okabe, M. Preparation and Characterization of Water Self-Dispersible Poly(3-hexylthiophene) Particles. *Polym. J.* **2008**, *40*, 33–36.
- (35) Rao, J. P.; Geckeler, K. E. Polymer Nanoparticles: Preparation Techniques and Size-Control Parameters. *Prog. Polym. Sci.* **2011**, *36*, 887–913.
- (36) Nagarjuna, G.; Baghgar, M.; Labastide, J.; Algaier, A. D. D.; Barnes, M. D.; Venkataraman, D. Tuning Aggregation of Poly(3-hexylthiophene) within Nanoparticles. *ACS Nano* **2012**, *6*, 10750–10758.
- (37) Ye, F.; Sun, W.; Zhang, Y.; Wu, C.; Zhang, X.; Yu, J.; Rong, Y.; Zhang, M.; Chiu, D. T. Single-Chain Semiconducting Polymer Dots. *Langmuir* **2015**, *31*, 499–505.
- (38) Wu, C.; Chiu, D. T. Highly Fluorescent Semiconducting Polymer Dots for Biology and Medicine. *Angew. chem. int. Ed.* **2013**, *52*, 3086–3109.
- (39) Prasad, K. P.; Than, A.; Li, N.; SK, M. A.; Duan, H.; Pu, K.; Zheng, X.; Chen, P. Thiophene-Derived Polymer Dots for Imaging Endocytic Compartments in Live Cells and Broad-Spectrum Bacterial Killing. *Mater. Chem. Front.* **2017**, *1*, 152–157.
- (40) Wu, C.; Szymanski, C.; McNeill, J. Preparation and Encapsulation of Highly Fluorescent Conjugated Polymer Nanoparticles. *Langmuir* **2006**, *22*, 2956–2960.

- (41) Lyon, J. E.; Cascio, A. J.; Beerbom, M. M.; Schlaf, R.; Zhu, Y.; Jenekhe, S. A. Photoemission Study of the Poly(3-hexylthiophene)/Au Interface. *Appl. Phys. Lett.* **2006**, *88*, 222109.
- (42) Scudiero, L.; Wei, H.; Eilers, H. Photoemission Spectroscopy and Atomic Force Microscopy Investigation of Vapor-Phase Codeposited Silver/Poly(3-hexylthiophene) Composites. *ACS Appl. Mater. Interfaces* **2009**, *1*, 2721.
- (43) Hintz, H.; Peisert, H.; Egelhaaf, H. J.; Chassé, T. Reversible and Irreversible Light-Induced p-Doping of P3HT by Oxygen Studied by Photoelectron Spectroscopy (XPS/UPS). *J. Phys. Chem. C* **2011**, *115*, 13373–13376.
- (44) Norrman, K.; Madsen, M. V.; Gevorgyan, S. A.; Krebs F. C. Degradation Patterns in Water and Oxygen of an Inverted Polymer Solar Cell. *J. Am. Chem. Soc.* **2010**, *132*, 16883–16892.
- (45) Oliva, M. M.; Casado, J.; López Navarrete, J. T.; Patchkovskii, S.; Goodson III, T.; Harpham, M. R.; Seixas de Melo, J. S.; Amir, E.; Rozen, S. Do [all]-S,S'-Dioxide Oligothiophenes Show Electronic and Optical Properties of Oligoenes and/or of Oligothiophenes?. *J. Am. Chem. Soc.* **2010**, *132*, 6231–6242.
- (46) Brown, P. J.; Thomas, D. S.; Köhler, A.; Wilson, J. S.; Kim, J.; Ramsdale, C. M.; Siringhaus, H.; Friend, R. H. Effect of Interchain Interactions on the Absorption and Emission of Poly(3-hexylthiophene). *Phys. Rev. B* **2003**, *67*, 064203.
- (47) Kurokawa, N.; Yoshikawa, H.; Hirota, N.; Hyodo, K.; Masuhara H. Size-Dependent Spectroscopic Properties and Thermochromic Behavior in Poly(substituted thiophene) Nanoparticles. *Chem. Phys. Chem.* **2004**, *5*, 1609–1615.
- (48) Labastide, J. A.; Baghgar, M.; Dujovne, I.; Venkatraman, B. H.; Ramsdell, D. C.; Venkataraman, D.; Barnes, M. D. Time- and Polarization-Resolved Photoluminescence of

Individual Semicrystalline Polythiophene (P3HT) Nanoparticles. *J. Phys. Chem. Lett.* **2011**, *2*, 2089–2093.

(49) Banerji, N.; Cowan, S.; Vauthey, E.; Heeger, A. J. Ultrafast Relaxation of the Poly(3-hexylthiophene) Emission Spectrum. *J. Phys. Chem. C* **2011**, *115*, 9726–9739.

(50) Bard, A. J.; Faulkner, L. R. *Electrochemical Methods: Fundamentals and Applications*; Wiley: New York, **1984**.

(51) Chaudhuri, R. G.; Paria, S. Core/Shell Nanoparticles: Classes, Properties, Synthesis Mechanisms, Characterization, and Applications. *Chem. Rev.* **2012**, *112*, 2373–2433.

(52) Melinon, P.; Begin-Colin, S.; Duvail J. L.; Gauffre, F.; Boime, N. B.; Ledoux, G.; Plain, J.; Reiss, P.; Silly, F.; Warot-Fonrose, B. Engineered Inorganic Core/Shell Nanoparticle. *Physics Reports* **2014**, *543*, 163–197.

(53) Melitz, W.; Jian Shen, J.; Kummel, A. C.; Lee, S. Kelvin probe force microscopy and its application. *Surf. Sci. Rep.* **2011**, *66*, 1–27.

(54) Baikie, I. D.; Mackenzie, S.; Estrup, P. J. Z.; Meyer, J. A. Noise and the Kelvin Method. *Rev. Sci. Instrum.* **1991**, *62*, 1326–1332.

(55) Baikie, I. D.; Venderbosch, E.; Meyer, J. A.; Estrup, P. J. Z. Analysis of Stray Capacitance in the Kelvin Method. *Rev. Sci. Instrum.* **1991**, *62*, 725–735.

(56) Liscio, A.; Palermo, E.; Fenwick, O.; Braun, S.; Mullen, K.; Fahlman, M.; Cacialli, F.; Samorì, P. Local Surface Potential of π -Conjugated Nanostructures by Kelvin Probe Force Microscopy: Effect of the Sampling Depth. *Small* **2011**, *7*, 634–639.

(57) Rozen, S.; Brand, M. A Novel Route for Epoxidation of Olefins Using Elemental Fluorine. *Angew. Chem. Int. Ed.* **1986**, *25*, 554–555.

(58) Dayan, S.; Kol, M.; Rozen, S. Tertiary Amine Oxidation using $\text{HOF}\cdot\text{CH}_3\text{CN}$: A Novel Synthesis of *N*-Oxides. *Synthesis* **1999**, 1427–1430.